ORIGINAL RESEARCH ARTICLE

Hot Corrosion Evaluation of Cr$_3$C$_2$/8YSZ-Based Plasma-Sprayed Coatings on SS316 in Na$_2$SO$_4$–V$_2$O$_5$ Molten Salt Environment at 700 °C

S. Maharajan [ORCID] · F. Michael Thomas Rex

Abstract Austenitic stainless steel used in power plants and chemical industries is susceptible to corrosion in high-temperature environments. The corrosion is accelerated in high-temperature applications due to chemical substances like sodium, sulfur, and vanadium. The current investigation involves the assessment of the hot corrosion performance of two distinct coatings, namely 8 wt.% yttria-stabilized zirconia (8YSZ) and chromium carbide (Cr$_3$C$_2$), which have been applied using air plasma spraying onto SS316. Coatings were analysed after being heated in the furnace for 50 h at 700 °C at 5 h/cycle with a salt mixture of Na$_2$SO$_4$− 60 wt.% of V$_2$O$_5$ (30 mg/cm^2). Elemental analysis of the hot corroded specimen was performed using scanning electron microscopy (SEM), x-ray diffraction analysis (XRD), and energy-dispersive spectroscopy (EDS). The findings indicate that the 8YSZ coating exhibited enhanced adherence to the substrate for the entire duration of the hot corrosion test. In contrast, it was observed that the Cr$_3$C$_2$ coating underwent total delamination subsequent to the fifth cycle of the hot corrosion test. Bare material shows a substantial degradation surface that peels off without substantial formation of strong surface adherence corrosion products.

Keywords Plasma spray coating · Hot corrosion · SS316 · Cr$_3$C$_2$ · 8YSZ

S. Maharajan (✉)
Mechanical Engineering, Ramco Institute of Technology, Rajapalayam 626117, India
e-mail: maharajan@ritrjpm.ac.in

F. M. T. Rex
Mechanical Engineering, National Engineering College, Kovilpatti 628503, India

Introduction

As a result of their exceptional mechanical properties and ability to resist corrosion under elevated temperatures, austenitic stainless steels find widespread application in various disciplines, such as power stations and nuclear power plants for pumps, tubes, and pipes. The primary cause of corrosion at elevated temperatures is the deposition of molten salts onto the surface of the components. The molten salts act as corrosive species that react with metal surfaces in a hot gas environment. Thus, coating on austenitic steel is highly preferable to counteract the deposited corrosive species and protect the components [1–5]. Plasma spray coating has shown to be an appropriate and cost-effective method for solving a wide range of issues in the manufacturing sector. These coatings allow significantly greater operation temperatures and higher efficiency [6, 7].

The coatings on superalloys have been performed by various researchers significantly. Deepa Mudugal et al. [8, 9] performed the Cr$_3$C$_2$-NiCr coating on Superni 600 alloy and ascertained that Cr$_3$C$_2$-based feedstock powders are the right choice for coatings in components used in high-temperature erosion and corrosion environments. The authors reported in [10–13] studied the the effects of elevated temperatures on chromium-based coatings applied to boiler steels and nickel-based superalloys, particularly when exposed to a corrosive hot salt environment and found the accumulation of NiO and Cr$_2$O$_3$ oxide layers on the coated surface. The existance of corrosion layer of oxide serves as an inhibitor to hinder the infiltration of the corrosive medium, hence impeding the oxidation of the entire coating. Alnaser [14] and Manpreet [15] analysed the failure mechanism of the Cr$_3$C$_2$-based coatings on nickel-

770

J Fail. Anal. and Preven. (2024) 24:769–778

based superalloy and boiler steel, respectively. The investigation revealed that the detachment and flaking off a oxide scales on the coated samples, when subjected to an environment consisting of molten salt at a temperature of 700 °C, may be attributable to the difference in the heat expansion coefficients among the coating, substrate and produced oxides. Sidhu et al. [16, 17] studied the crucial aspects of cyclic corrosion of the Cr_3C_2-based coatings at high temperature on high-performance materials in Na_2SO_4-V_2O_5 salt combination at 900 °C. At the outset, the coatings experienced a substantial oxidation rate, because the oxidizing species could get into the splat borders and open pores and quickly form oxides in the pores. Kuruba et al. [18] investigated the hot corrosion performance of Cr_3C_2/carbon nanotubes composite coatings on boiler tube steels in molten salt conditions and the study demonstrated that including 7 wt.% of carbon nanotubes (CNTs) into the Cr_3C_2 feedstock powder yielded excellent substrate adherence.

Substantial research work has also been reported on the effectiveness of YSZ coating in resisting corrosion at elevated temperatures for various substrate materials. YSZ has been recognized as a desirable material for applications involving elevated temperatures. It makes the scale stick to the alloy substrate better, which makes the metal more resistant to thermal cycles. Dharuman et al. [19] and Dinesh et al. [20] analysed the failure mechanism of hot corroded coated steel in molten salt. More acidic stabilizers can delay or prevent the change of zirconia to completely monoclinic, which is the cause of YSZ's failure. Coatings made of YSZ were shown to be the most effective coatings in thermal barrier characteristics of gas turbine blades, and their hot corrosion behavior on superalloys in hot gas environments has been reported in the previous work [21–26]. The study conducted by Avci et al. [27] examined the effectiveness of YSZ coating in preventing corrosion at high temperatures. Yttrium vanadate (YVO_4) was found to be generated as a result of the interaction between yttria and vanadium pentoxide (V_2O_5) at high-temperature conditions. Further studies reported that the formation of oxides efficiently suppressed the spallation of top coatings, microcracking, and tiny fractures in early cycles. Spallation causes a little weight loss in YSZ coatings, whereas the thermal growth of oxides adds an incremental amount of weight. Therefore, it displays the characteristic of a widening diffusion-controlled region during prolonged heating cycles in the melting salt conditions.

The available literature indicates a limited amount of research conducted on the subject of hot corrosion in austenite steel, despite its extensive use in high-temperature environments in industry. In practical scenarios, the material undergoes prolonged exposure to a high-temperature gaseous environment. However, most literature studies revealed that hot corrosion testing occurs within 1 h of exposure. Hence, it is important to test the coatings in extended exposure time in a hot environment for 5 h in our study and cool in a furnace for 1 h for each cycle. The extensive literature study reveals that both coatings are comparatively competent in hot corrosion resistance. Though substantial work has been done to assess the effectiveness of various thermal spray coatings in both atmospheric and saline conditions through laboratory experimentation, the necessity of evaluating the extreme temperatures corrosion resistance of carbide coatings with oxide coatings for applications requiring elevated temperatures of austenitic stainless steel remains. The present study compares uncoated, Cr_3C_2, and 8YSZ plasma-sprayed austenitic stainless steel's corrosion performance in a heated environment in a Na_2SO_4—60 wt.% V_2O_5 molten salt conditions at 700 °C for 10 cycles. The examination of corrosion products is performed by the application of scanning electron microscopy (SEM), energy-dispersive x-ray analysis (EDAX), and x-ray diffraction (XRD) techniques.

Experimental Procedure

Substrate Material and Coatings

The rectangular form of hot-rolled annealed sheet of austenitic stainless steel (SS316) has been procured from Metal World, Chennai, India. The elemental composition (wt.%) of the austenitic stainless steel (SS316) is 0.08 C, 0.1 N, 18.4 Cr, 12.52 Ni, 2.1 Mo, 1.8 Mn, 0.75 Si, 0.01 S, 0.03 P, 0.4 Cu, and the remaining Fe. The substrate has been machined to dimensions of 25 × 25 × 5 mm in the EDM machine. The commercially available Cr_3C_2 powder and 8YSZ with a 25–40 μm particle size are used as feedstock-coated materials on the substrate using the plasma spray coating process. To eliminate any existing thin oxide coating or scale on the specimen, the polishing process entailed employing emery paper with several grit levels, including 220, 320, 400, 600, and 800 and then, a cloth was used to polish with a suspension of alumina powder. After cleaning with acetone, The specimens underwent grit blasting using alumina powder with an average particle size of 25 μm before coating the substrate. A bond coating with a thickness of 50 μm, consisting of a nickel-chromium (Ni-Cr) alloy in an 80:20 wt.% ratio, was applied. The intended top coatings were made with the thickness of 200 μm on the substrate.

High-Temperature Corrosion Experimental Process

Comparative investigations were performed on both bare material and coated specimens to examine the phenomenon of hot corrosion. The substrates underwent a washing process using distilled water, followed by a cleaning using acetone. The samples were further subjected to a temperature of 230 °C within the furnace, both before to and subsequent to the application of the salt suspension. The salt slurry consisting of Na_2SO_4 and 60 wt.% V_2O_5 was made by completely blending it with distilled water. A homogeneous coating of the slurry, measuring 30 mg/cm^2, was then applied to the samples. The specimens underwent cyclic hot corrosion in a furnace at a temperature of 700 °C for a total of 10 cycles. Each iteration included of a 5-h period of heating, succeeded by a 30-min interval of cooling in the surrounding atmospheric conditions. Throughout the course of the experimental method, each individual sample was carefully placed into an alumina crucible, and subsequently, the collective mass of the crucible and the specimen was determined. The starting weight of the sample was recorded and subsequently, the weight change was documented after each cycle utilizing a weighing scale with an accuracy of 1 mg. These data were utilized to establish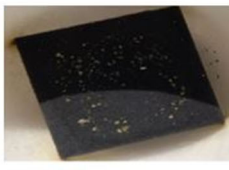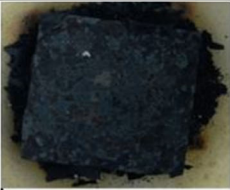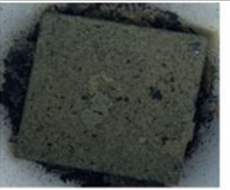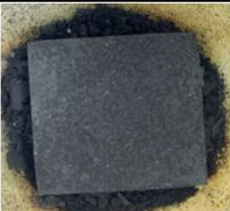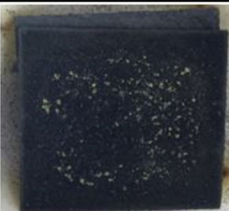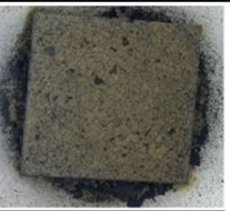 the corrosion kinetics based on the observed weight changes. The inclusion of the spalled scale during the weight change measurement was undertaken to ascertain the comprehensive corrosion rate.
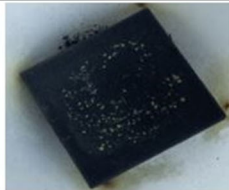
Results and Discussion

Macro-Image Study of Hot Corroded Samples

Figure 1 displays the macroscopic pictures of the hot corroded specimens in a crucible after the first, fifth, and tenth cycle in a Na_2SO_4–60 wt.%V_2O_5 molten salt solution at a temperature of 700^{0}C, under various cyclic circumstances. A grayscale with brown spots emerged in the uncoated sample in the first cycle as shown in Fig. 1a. After the first cycle, the surfaces of the specimen developed a delicate scale. At the end of the fifth cycles, the scales began to peel off the surfaces because they were too fragile to hold on as evidenced. The spallation persisted until the end of the investigation. As the investigation progressed, the oxide scale displayed a growing prevalence of brown spots on a gray backdrop. More dark gray-colored powder particles were spilt inside the crucible. Upon observing the Cr_3C_2-coated specimen as shown in Fig. 1b, the color changed to dark gray with light green dots at the starting stage, along

Fig. 1 Macro-hot corroded images of (**a**) SS316 substrate (**b**) Cr_3C_2-coated (**c**) 8YSZ-coated in crucible after 1st, 5th and 10th cycle in Na_2SO_4 – 60 wt.%V_2O_5 molten salt solution at 700 °C

772

J Fail. Anal. and Preven. (2024) 24:769–778

with the appearance of dispersed brown salt crystals. After the completion of the fifth cycle, a little amount of spallation in powder form was seen within the crucible. The oxide scale exhibited a dark green hue. Subsequently, as the exposure continued, the coloration gradually shifted toward a dark gray backdrop, accompanied by a dispersed bright green pattern. Upon the completion of 10 cycles, as shown in Fig. 1b, the scale exhibited a mostly black coloration with sporadic hints of greenish hues. In 8YSZ-coated sample as shown in Fig. 1c, spallation of yellow-colored layer debris has been formed and detached on the surface for the first five cycles. Minute cracks appeared and progressed to form the oxide scales. More debris was formed after the fifth cycle. No further detachments occurred after the fifth cycle to the tenth cycle. However, a dark gray appearance has been found after the eighth to tenth cycle. More minute cracks appeared without spallation of the oxide scale. A loose structure has been identified. Significant light yellow-colored oxide scale particles fell inside the crucible.

Corrosion Kinetics

Figure 2a displays the weight gain per unit area (mg/cm^2) plotted against time for both bare and coated specimens, presented in multiple cycles. The hot corrosion rate constant shown in Table 1 has been measured from the graph (weight gain/area)^2 vs. exposure time as debicted in Fig. 2b. The weight gain/area for Cr_3C_2-, 8YSZ-coated, and uncoated are 40.224 mg/cm^2, 14.368 mg/cm^2, and 19.56 mg/cm^2 upon the completion of 10 cycles. Significant increase in mass was experienced in the Cr_3C_2-coated specimen in comparison with the 8YSZ-coated and uncoated specimens. The 8YSZ coating exhibited a rate of oxidation that precisely followed a parabolic in nature, while the Cr_3C_2 coatings demonstrated the highest linear rate of oxidation. The Cr_3C_2 coating exhibits a coefficient of determination (R^2) value of 0.95, indicating that it adheres to the linear rate of the law of oxidation by 95% and the parabolic rate by 5%. On the other hand, the 8YSZ coating displays an R^2 value of 0.51, suggesting that it predominantly adheres to the parabolic rate law with a 49% contribution from the linear rate [8]. Hence, 8YSZ exhibited high diffusion-controlled behavior of oxidation. The material coated with 8YSZ has effectively mitigated hot corrosion due to the congestion of corrosion products on the upper surface that remain adhered to the coated material. Due to the entry of corrosive media into coatings, oxides rapidly develop at splat boundaries and in open pores, increasing their initial corrosion rate. Oxides clogged holes and splat boundaries in coatings, preventing additional corrosive media penetration.

In the case of the uncoated material, the surface is substantially destructed, and the surface materials are peeling off significantly. Corrosion products formed during the cyclic heat exposure investigation resulted in a substantial mass gain. Uncoated material has $R^2 = 0.93$, indicating the 93% linear rate of oxidation.

Table 1 Parabolic rate constant (K_p) (10^{-6} g^2/cm^4/s)

Sample	Hot corrosion at molten salt at 700 °C (g^2/cm^4/s)
Uncoated	7.64
Cr_3C_2-coated	34.17
8YSZ-coated	2.99
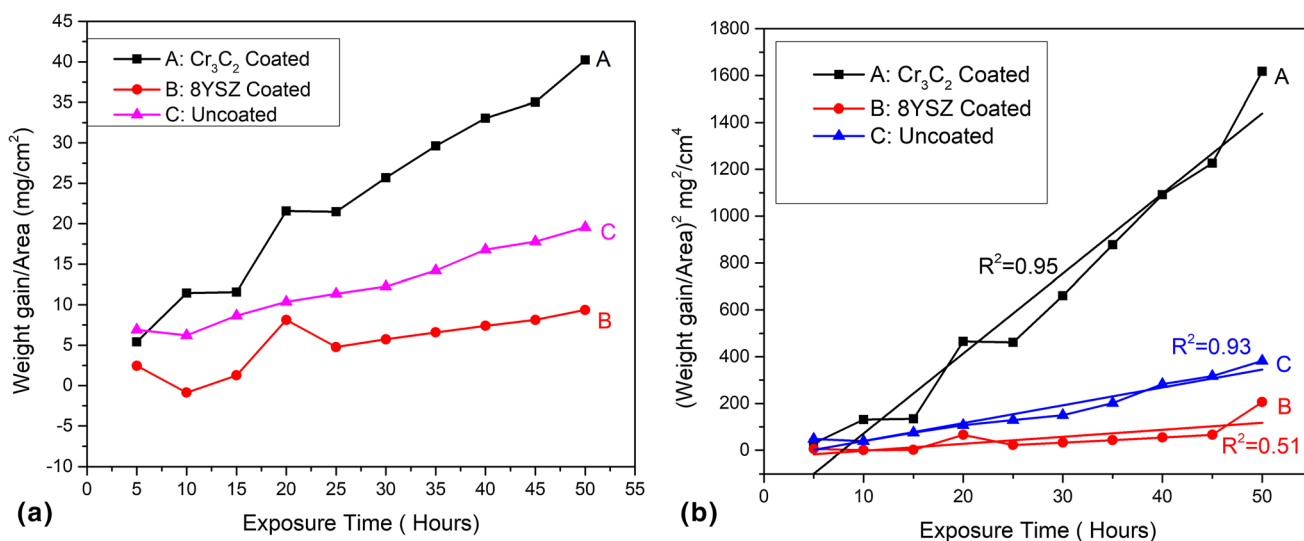
Fig. 2 (a) Weight gain/Area (mg/cm^2) Vs Exposure Time (Hours), (b) (Weight gain/ Area)^2 (mg^2/cm^4)Vs. Exposure Time (Hours) for bare, Cr_3C_2- and 8 YSZ-coated specimen subjected to hot corrosion for 10 cycles in Na$_2$SO$_4$ + 60 wt.% V$_2$O$_5$ environment at 700 °C

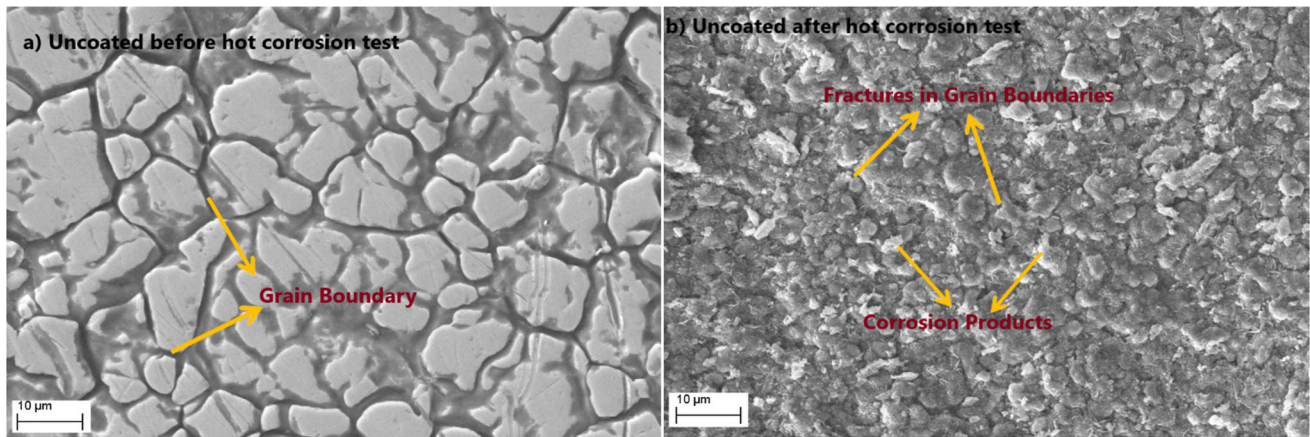J Fail. Anal. and Preven. (2024) 24:769–778

773

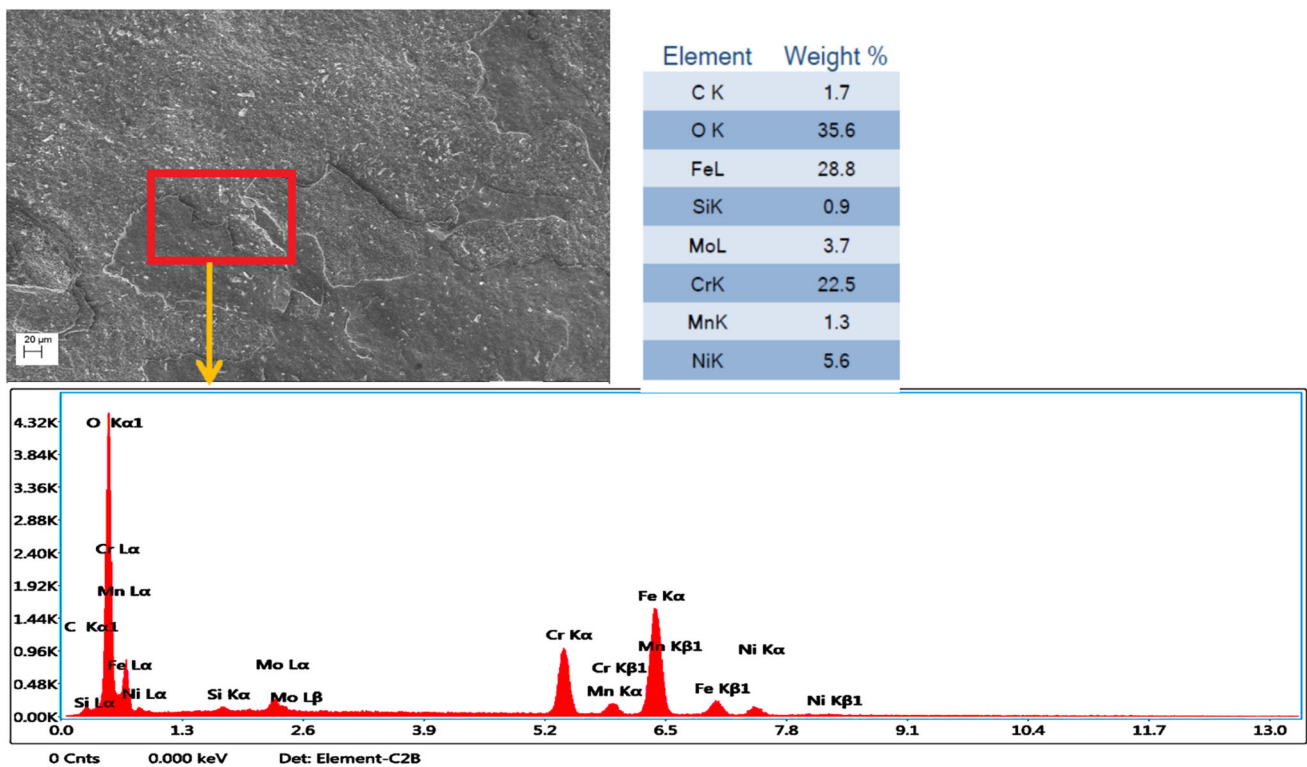Fig. 3 SEM analysis of (a) uncoated sample before hot corrosion, (b) after hot corrosion

Fig. 4 EDAX analysis of hot corroded uncoated sample

SEM/EDAX and XRD Analysis of Hot Corroded Samples

Figure 3 reveals the surface morphology of (a) uncoated sample before hot corrosion and (b) after hot corrosion under 50 h of exposure in the hot salt condtions at 700 °C for ten cycles. The oxide scales, porosity in the form of round pits, and many fractures with tiny white flakes are visible. The EDAX analysis (Fig. 4) of a hot corroded uncoated sample reveals the chemical elements O, Cr, Fe, Ni, and Mo. The oxygen (O) element increases due to loose nonproductive oxide scales forming in white patches [8]. Equation 1 depicts the solid phase interaction between Cr_2O_3 and NiO that led to the creation of $NiCr_2O_4$ flakes.

$$Cr_2O_3 + NiO \rightarrow NiCr_2O_4 \tag{Eq 1}$$

The XRD analysis (Fig. 5) of hot corroded uncoated SS316 consists of Fe_2O_3 and $NiCr_2O_4$. The reaction makes the oxide scale grow and dissolve simultaneously in the

774

J Fail. Anal. and Preven. (2024) 24:769–778

liquid salt. The observed strong spalling of the uncoated steel scale might potentially be interpreted due to the tremendous strain caused by Fe_2O_3 settling out of the liquid and the diffusion between iron oxide's middle layers.

Figure 6 shows the sample of (a) Cr_3C_2-coated before hot corrosion and (b) after hot corrosion under 50 h of exposure in the molten salt conditions at 700 °C for ten cycles. Figure 7 depicts an EDAX representation that exhibits the occurrence of oxygen (O), chromium (Cr), and nickel (Ni) throughout the process of spinel structure creation. Cr and O may be seen in the needle or platelet oxide. Cr and O combine to generate Cr_2O_3, which takes on a platelet-like shape. Large gray-black particles began to settle in and around the gaps in the coating's surface. The predominant constituents of the substantial gray particles
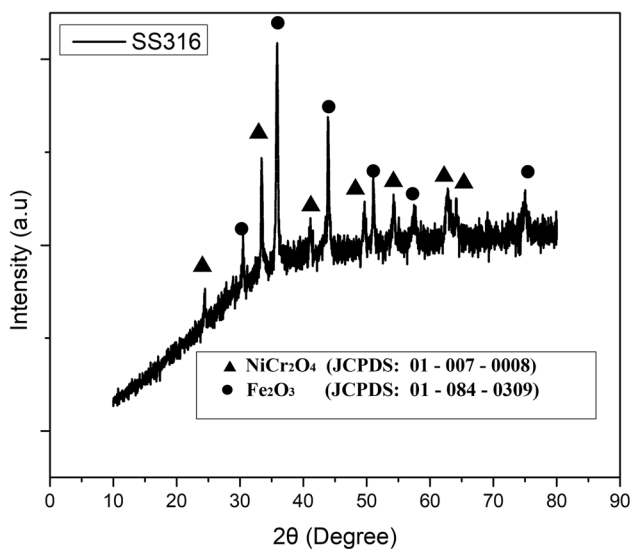
Fig. 5 XRD analysis of hot corroded bare SS316

include elements such as chromium (Cr), oxygen (O), nickel (Ni), sodium (Na), and sulfur (S). These particles are likely to consist of incomplete sodium sulfate (Na_2SO_4) salts and oxides that contain nickel and chromium components. At temperatures above 700 °C, a significant reduction in density occurred on the coated surface, accompanied by the expansion of particulate structures into platelike crystals composed of chromium (Cr) and oxygen (O) components. The aforementioned study findings suggest that the Na_2SO_4 salt had a pronounced corrosive impact on the Cr_3C_2 coating. When hot corrosion temperatures increased, the damage produced by coating corrosion became more severe [12].

The XRD analysis of the hot corroded Cr_3C_2-coated sample is shown in Fig. 8. The analysis demonstrates the presence of notable phases such as chromium(III) oxide (Cr_2O_3), iron-nickel sulfide (($Fe, Ni) S_2$), and sodium sulfate (Na_2SO_4). The coated specimens exhibit a notable rise in weight during the early five cycles of hot corrosion, followed by a more steady increase in weight growth thereafter. The observed increase in weight of the specimens during the initial cycles might perhaps be attributed to the development of oxides of each active element included within the coating. Subsequently, the oxidation rate exhibits a progressive rise as a result of the emergence of productive oxide scales entitled Cr_2O_3 and ($Fe, Ni) S_2$, which effectively impede the flow of oxygen or other corrosive elements. However, due to temperature cycles, the oxides generated on the top of the coatings may spall or peel, especially around the edges of the specimens. The underlying cause of this phenomenon may be ascribed to the disparate rate of thermal expansion shown by the substrate and the coating. The presence of fragmentation might perhaps be ascribed to the swift occurrence of fractures in the proximity of coating bulges. This phenomenon occurs due to the tensile radial stress that
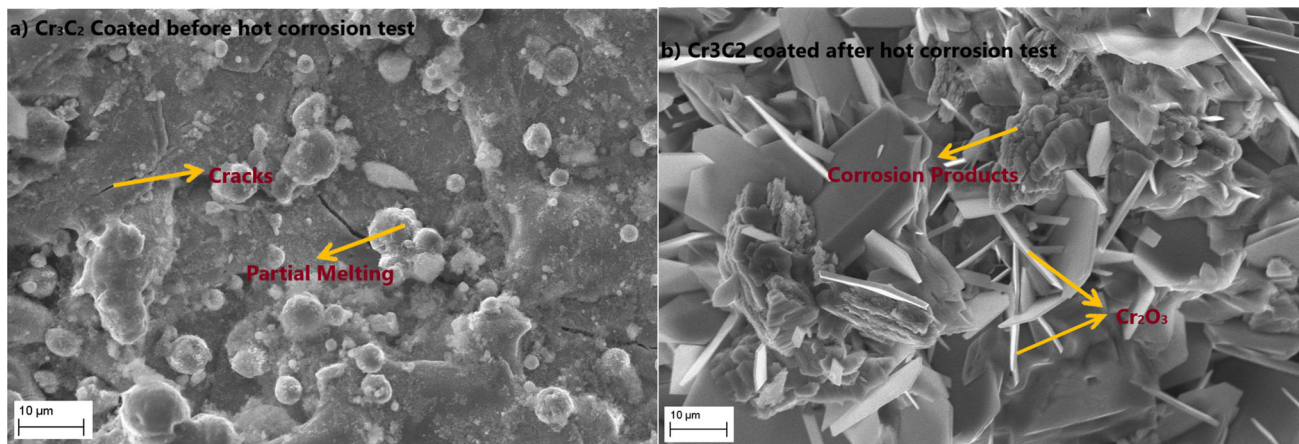
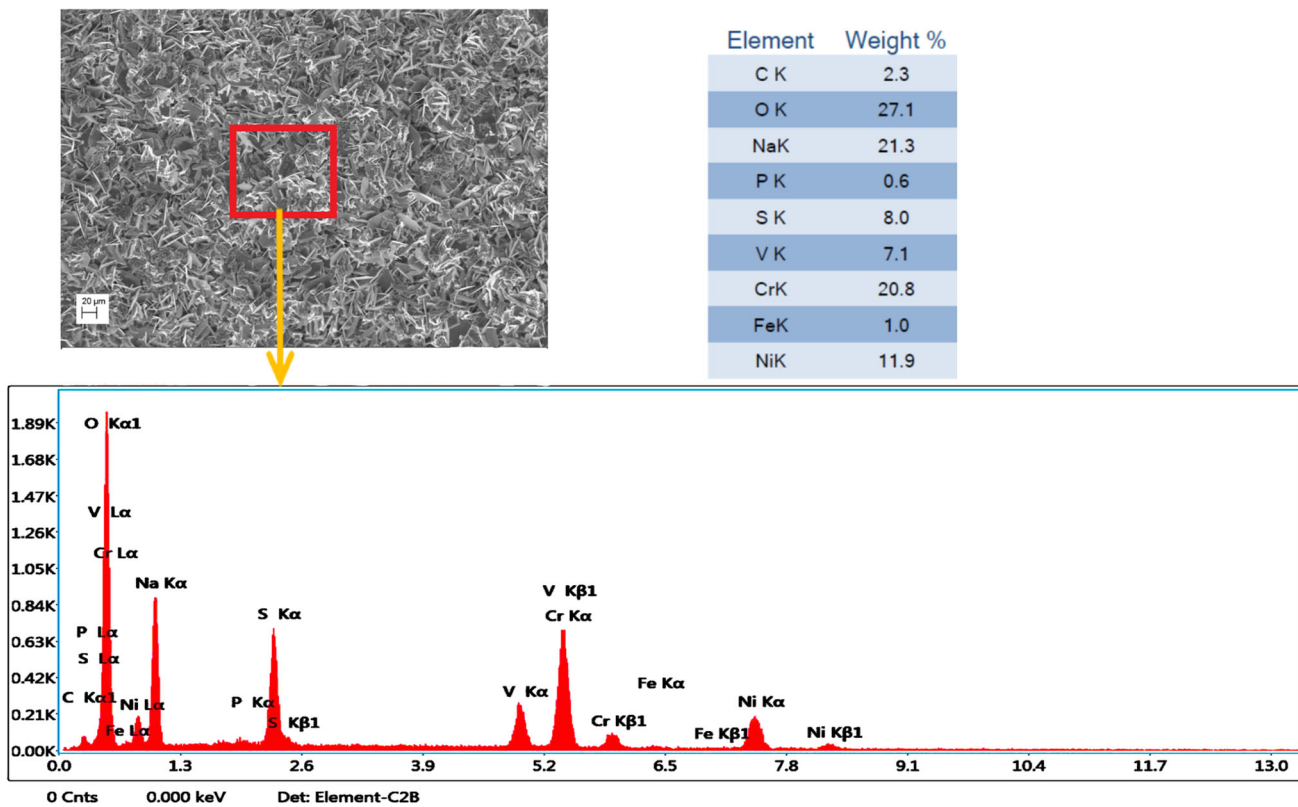Fig. 6 SEM analysis of (a) Cr_3C_2-coated sample before hot corrosion, (b) after hot corrosion

Fig. 7 EDAX analysis of hot corroded Cr_3C_2-coated sample
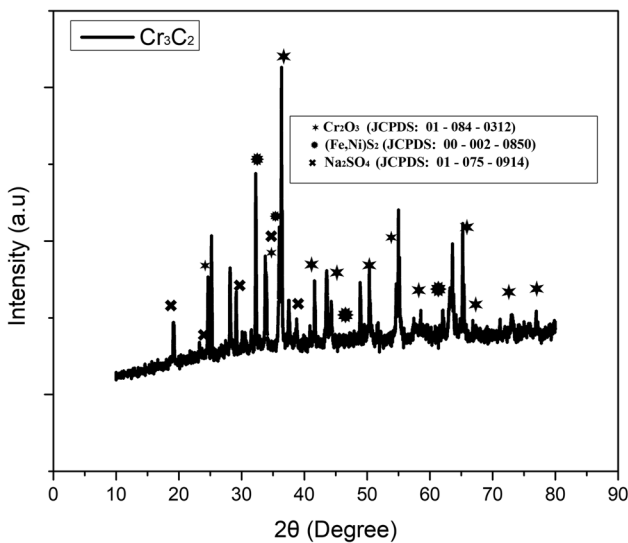

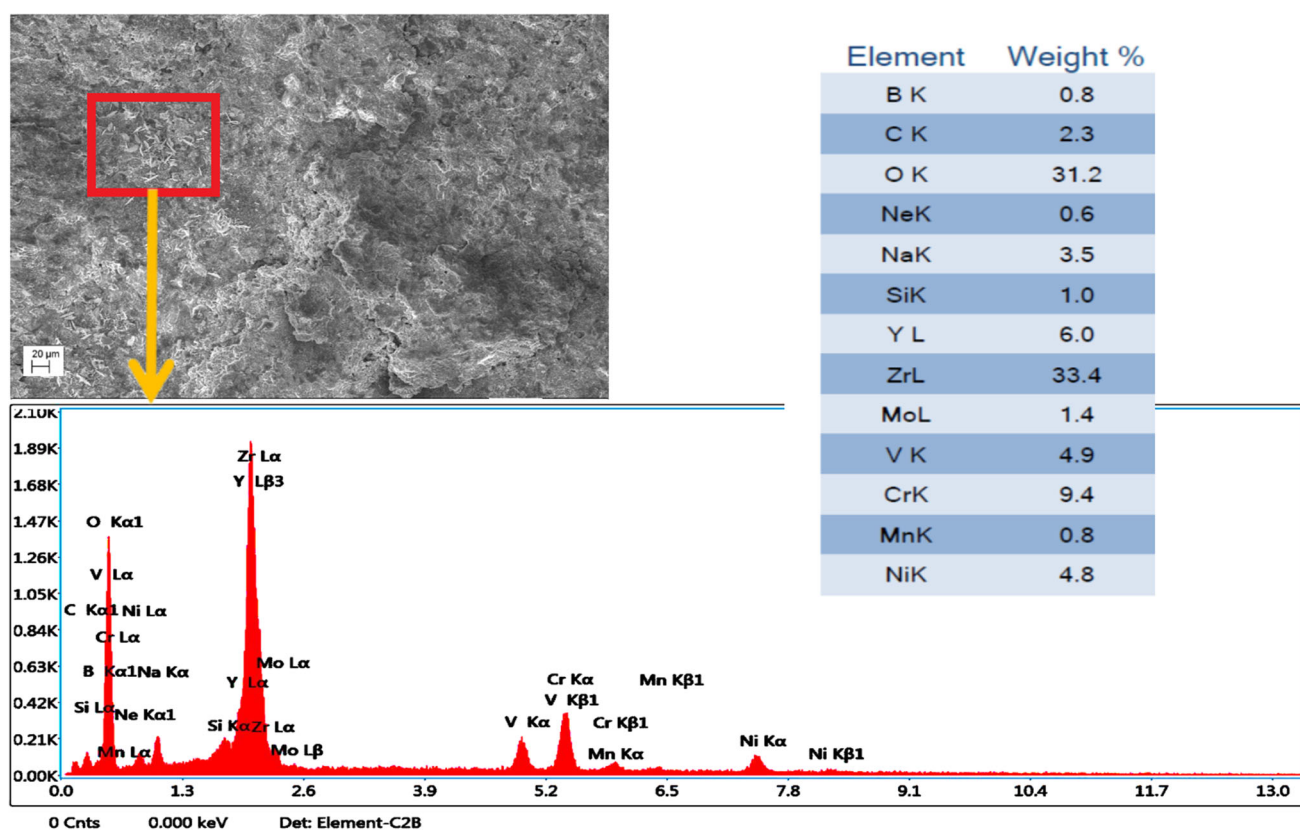**Fig. 8** XRD analysis of hot corroded Cr_3C_2 coating

emerges during the cooling process, which is caused by the notable difference in thermal contraction between the oxide and the coating material. Fractures are formed inside the coating due to the existence of stress within the deposit or at the interface between the coating and the substrate metal [16, 17].

Figure 9 shows the surface morphology of the sample (a) 8YSZ-coated before hot corrosion and (b) after hot corrosion under 50 h of exposure for ten cycles in the molten salt environment at 700 °C. The EDAX analysis (Fig. 10) reveals the major elements Zr, V, Y, Na, O, and a small amount of Ni and Cr. Because of the thermal stress generated by rod crystals and the change from tetragonal to monoclinic zirconia, the salt interacts with the YSZ layer, resulting in the disintegration and delamination of the zirconia coating. Two distinct phases were present in the corrosion by-products: YVO_4 on the outside and monoclinic zirconia on the inside. During exposure, the 40% Na_2SO_4 and 60% V_2O_5 in the salt mixture interacted to form the eutectic compound Na_2VO_3. The Na_2VO_3 molecule carried oxygen while also acting as a corrosion catalyst. The substance, intended to permeate the coating's pores, aggressively interacted with Y_2O_3, creating YVO_4 and ZrO_2.

The peaks of monoclinic ZrO_2 peaks and YVO_4 spinels were observed in an XRD study (Fig. 11) of a hot corroded 8YSZ-coated sample.
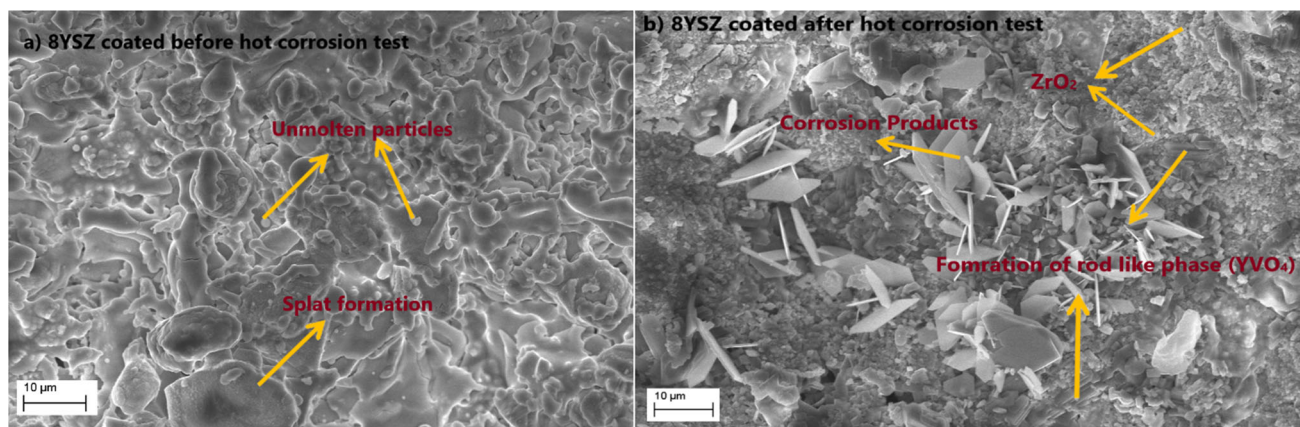
Fig. 9 SEM analysis of (a) 8YSZ-coated sample before hot corrosion, (b) after hot corrosion

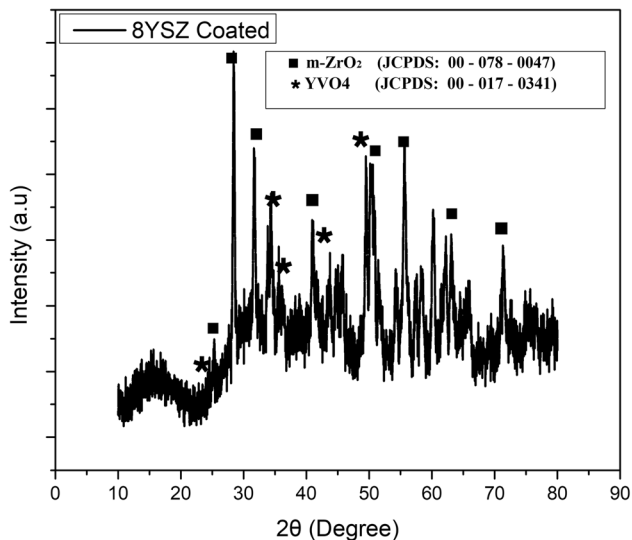Fig. 10 EDAX analysis of hot corroded 8YSZ sample

Conclusion

The investigation involved conducting hot corrosion experiments on SS316 samples with three different coatings: uncoated, Cr_3C_2-coated, and 8YSZ-coated. These experiments were carried out in a molten salt environment consisting of Na_2SO_4 (sodium sulfate) and 60% by weight V_2O_5 (vanadium pentoxide). The samples were exposed to this environment at a temperature of 700 °C for a total

duration of 50 h, with each cycle lasting 5 h. The following findings has been observed,

a. The bare materials demonstrated notable spallation, accompanied by the formation of loosely attached oxide scales and tiny particles, such as Fe_2O_3 and Ni_2CrO_4.

b. The stainless steel SS316 coated with Cr_3C_2 experienced complete delamination after the completion of the tenth cycle. The heat cycle led to the detachment

Fig. 11 XRD analysis of hot corroded 8YSZ Coating

due to surface degradation or delamination of the oxides that had grown on the surface of the Cr_3C_2-coatingsThe aforementioned phenomena was prominently seen in the vicinity of the specimens' boundaries, maybe as a result of the disparity in thermal expansion coefficients between the coatings and the substrate.

c. The stainless steel SS316 coated with 8YSZ demonstrated enhanced resistance to heat corrosion, assuming that the predominant composition of the scale formed is mostly ZrO_2 and YVO_4. Following the completion of the tenth cycle, it can be observed that the coating has finely adhered to the substrate with little fragmentation of coated particles.

References

1. P.S. Rajendran, High temperature corrosion of austenitic stainless steels, in H.S. Khatak, B. Raj (eds.), *Woodhead Publishing Series in Metals and Surface Engineering. Corrosion of Austenitic Stainless Steels*, pp. 265–286 (2002). https://doi.org/10.1533/9780857094018.287

2. Z. Lin, P. Ren, R. Zhu, X. Tang, Y. Zheng, T. Xu, Y. Wang, J. Yang, J. Cai, The effect of molten phosphate on corrosion of 316 stainless steel, alloy 625, and titanium TA8 in supercritical water oxidation conditions. Materials. **16**, 395 (2023). https://doi.org/10.3390/ma16010395

3. G.M. Yi, Y.H. Cheng, L. Ren, J. Yang, Q. Wang, X. Li, Corrosion behavior of 316 stainless steel for advanced high-temperature water-cooled nuclear plant. Surf. Interface Anal. **54**(7), 767–774 (2022). https://doi.org/10.1002/sia.7089

4. H. Zhou, Z. Tian, C. Liao, Corrosion behaviour characterization of 316L stainless steel and Inconel 625 in supercritical water containing hydrochloric acid and high oxygen. Corros. Eng. Sci. Technol.. Eng. Sci. Technol. **57**(7), 640–647 (2022). https://doi.org/10.1080/1478422X.2022.2112931

5. X. Huang, K. Xiao, X. Fang, Z. Xiong, L. Wei, P. Zhu, X. Li, Oxidation behavior of 316L austenitic stainless steel in high temperature air with long-term exposure. Mater. Res. Express. **7**(6), 066517 (2020). https://doi.org/10.1088/2053-1591/ab96fa

6. R. Vaben, E. Bakan, D.E. Mack, A perspective on thermally sprayed thermal barrier coatings: current status and trends. J. Therm. Spray Tech. **31**, 685–698 (2022). https://doi.org/10.1007/s11666-022-01330-2

7. H. Singh, B.S. Sidhu, D. Puri, S. Prakash, Use of plasma spray technology for deposition of high temperature oxidation/corrosion resistant coatings—a review. Mater. Corros.Corros. **58**(2), 92–102 (2007). https://doi.org/10.1002/maco.200603985

8. D. Mudgal, S. Kumar, S. Singh, S. Prakash, Corrosion behavior of bare, Cr_3C_2-25%(NiCr), and Cr_3C_2-25%(NiCr) + 0.4%CeO_2—coated Superni 600 under molten salt at 900 °C. J. Mater. Eng. Perform. **23**, 3805–3818 (2014). https://doi.org/10.1007/s11665-014-1177-3

9. D. Mudgal, S. Singh, S. Prakash, Hot corrosion behavior of bare, Cr_3C_2-(NiCr) and Cr_3C_2-(NiCr) + 0.2 wt.% Zr coated SuperNi 718 at 900 °C. J. Mater. Eng. Perform. **24**, 1–15 (2015). https://doi.org/10.1007/s11665-014-1279-y

10. H. Singh, M. Kaur, S. Prakash, High-temperature exposure studies of HVOF-sprayed Cr_3C_2-25(NiCr)/(WC-Co) coating. J. Therm. Spray Technol. **25**, 1192–1207 (2016). https://doi.org/10.1007/s11666-016-0424-6

11. K. Lencova, F. Netrvalova, M. Vostrak, M. Lukac, F.R. Musalek, esanek C, Houdkova ZS, Hot corrosion behavior of TWAS and HVOF NiCr-based coatings in molten salt. Materials. **16**, 1712 (2023). https://doi.org/10.3390/ma16041712

12. M. Shi, Z. Xue, H. Liang, Z. Yan, X. Liu, S. Zhang, High velocity oxygen fuel sprayed Cr_3C_2-NiCr coatings against Na_2SO_4 hot corrosion at different temperatures. Ceram. Int. **46**(15), 23629–23635 (2020). https://doi.org/10.1016/j.ceramint.2020.06.135

13. S. Saladi, J. Menghani, S. Prakash, Hot corrosion behaviour of detonation-gun sprayed Cr_3C_2–NiCr coating on inconel-718 in molten salt environment at 900 °C. Trans. Indian Inst. Met. **67**, 623–627 (2014). https://doi.org/10.1007/s12666-014-0383-x

14. I.A. Alnaser, M. Yunus, R. Alfattani, T. Alamro, High-temperature corrosion of APS and HVOF-coated nickel-based super alloy under air oxidation and melted salt domains. Materials. **14**, 5119 (2021). https://doi.org/10.3390/ma14185119

15. M. Kaur, H. Singh, S. Prakash, High-temperature corrosion studies of HVOF-sprayed Cr_3C_2-NiCr coating on SAE-347H boiler steel. J. Therm. Spray Technol. **18**, 619–632 (2009). https://doi.org/10.1007/s11666-009-9371-9

16. T.S. Sidhu, S. Prakash, R.D. Agrawal, Performance of high-velocity oxyfuel-sprayed coatings on an Fe-based superalloy in Na_2SO_4-60%V_2O_5 environment at 900 °C part II: hot corrosion behavior of the coatings. J. Mater. Eng. Perform. **15**, 130–138 (2006). https://doi.org/10.1361/105994906X83411

17. T.S. Sidhu, S. Prakash, R.D. Agrawal, Characterizations and hot corrosion resistance of Cr_3C_2-NiCr coating on Ni-base superalloys in an aggressive environment. J. Therm. Spray Tech. **15**, 811–816 (2006). https://doi.org/10.1361/105996306X147162

18. M. Kuruba, G. Gaikwad, D. Shivalingappa, Hot-corrosion behaviour of CNT reinforced Cr_3C_2-NiCr coatings working under high-temperature sprayed by HVOF method. Proc. Inst. Mech. Eng. L. (2022). https://doi.org/10.1177/14644207221082237

19. N. Dharuman, M. Arulmozhi, M.S. Babu, Investigations on oxidation, hot corrosion and thermal gradient performance of low k-$La_2Mo_2O_9$ thermal barrier coating. Bull. Mater. Sci. **44**, 8 (2021). https://doi.org/10.1007/s12034-020-02279-0

20. D. Gond, D. Puri, S. Prakash, Hot corrosion behaviour of yttria-stabilized zirconia as plasma sprayed coated boiler steel in air and salt at 900 °C under cyclic condition. J. Min. Mater. Charact. Eng. **10**(5), 463–478 (2011). https://doi.org/10.4236/jmmce.2012.113021

21. N. Ejaz, L. Ali, F. Ahmed, G. Awan, K.M.A. Ghauri, Hot corrosion behavior of double ceramic layered $CaZrO_3$/Yttria-stabilized zirconia coatings. Int. J. Appl. Ceram. **15**(1), 53–62 (2018). https://doi.org/10.1111/ijac.12767

22. A.G. Gonzalez-Hernandez, H. Ageorges, M.E. Lopez-Gomez, Evaluation of hot corrosion of 8YSZ coatings elaborated by suspension plasma spraying. J. Phys. Conf. Ser. **786**(01), 0112018 (2017). https://doi.org/10.1088/1742-6596/786/1/012018

23. H. Habibi, S. Guo, Evolution of hot corrosion behavior of YSZ-Ta_2O_5 composites with different YSZ/Ta_2O_5 ratios. Int. J. Appl. Ceram. **12**(3), 542–550 (2015). https://doi.org/10.1111/ijac.12224

24. I.N. Qureshi, M. Shahid, N.A. Nusair Khan, Hot corrosion of yttria-stabilized zirconia coating, in a mixture of sodium sulfate and vanadium oxide at 950 °C. J. Therm. Spray Tech. **25**, 567–579 (2016). https://doi.org/10.1007/s11666-015-0374-4

25. M. Karabaş, E. Bal, Y. Taptik, Hot corrosion behaviour of plasma sprayed alumina + YSZ particle composite coating. Prot. Met. Phys. Chem. Surf. **53**, 859–863 (2017). https://doi.org/10.1134/S2070205117050069

26. K.P. Jonnalagadda, S. Mahade, N. Curry, Hot corrosion mechanism in multi-layer suspension plasma sprayed $Gd_2Zr_2O_7$/YSZ thermal barrier coatings in the presence of V_2O_5 + Na_2SO_4. J. Therm. Spray Tech. **26**, 140–149 (2017). https://doi.org/10.1007/s11666-016-0486-5

27. A. Avci, M. Karabaş, A. Akdogan Eker, E. Akman, C. Aslan, Hot corrosion and CMAS degradation of laser-glazed YSZ coating with optimum parameter. Proc. Inst. Mech. Eng. L. (2023). https://doi.org/10.1177/14644207231178174